A prism based magnifying hyperlens with broad-band imaging

Habib, Md. Samiul; Stefani, Alessio ; Atakaramians, Shaghik; Fleming, Simon C.; Argyros, Alexander; Kuhlmey, Boris T.

Published in:
Applied Physics Letters

Link to article, DOI:
10.1063/1.4978445

Publication date:
2017

Document Version
Peer reviewed version

A prism based magnifying hyperlens with broad-band imaging

Md. Samiul Habib,[1, a)] Alessio Stefani,[1, 2] Shaghik Atakaramians,[1] Simon C. Fleming,[1] Alexander Argyros,[1] and Boris T. Kuhlmey[1, 3]

[1)]*Institute of Photonics and Optical Science (IPOS), School of Physics, The University of Sydney, Sydney, New South Wales, 2006, Australia*

[2)]*DTU Fotonik, Department of Photonics Engineering, Technical University of Denmark, DK-2800 Kgs. Lyngby, Denmark*

[3)]*Centre for Ultrahigh Bandwidth Devices for Optical Systems (CUDOS), School of Physics, Sydney, The University of Sydney, New South Wales, 2006, Australia*

Magnification in metamaterial hyperlenses has been demonstrated using curved geometries or tapered devices, at frequencies ranging from the microwave to the ultraviolet spectrum. One of the main issues of such hyperlenses is the difficulty in manufacturing. In this letter, we numerically and experimentally study a wire medium prism as an imaging device at THz frequencies. We characterize the transmission of the image of two sub-wavelength apertures, observing that our device is capable of resolving the apertures and producing a two-fold magnified image at the output. The hyperlens shows strong frequency dependent artefacts, a priori limiting the use of the device for broad-band imaging. We identify the main source of image aberration as the reflections supported by the wire medium, and also show that even the weaker reflections severely affect the imaging quality. In order to correct for the reflections, we devise a filtering technique equivalent to spatially variable time gating so that ultra-broad band imaging is achieved.

One of the fundamental limitation of conventional imaging systems is the diffraction limit, which arises due to high spatial frequencies rapidly decaying in conventional materials, preventing sub-wavelength features being transmitted in the far-field.[1] Hyperbolic metamaterials offer a solution to overcome the diffraction limit: they have large anisotropy resulting in a hyperbolic dispersion relation.[2,3] This specific property allows the propagation of extraordinary waves containing the information of high spatial frequencies. Owing to this, images can be transmitted over several wavelengths with no loss of information.[3] Up to now, a number of theoretical and experimental implementations of magnifying hyperlenses have been realized for frequencies ranging from microwave to ultraviolet.[4–13] In order to magnify images to the far-field, a curved geometry based hyperlens was proposed in 2006, with sub-wavelength alternating layers of metal and dielectric in a cylindrical geometry.[4,5] Such a metamaterial based hyperlens supports high spatial frequency propagating extraordinary waves, and due to the cylindrical geometry high transverse wave vectors are compressed, resulting in a magnified image at the output of the hyperlens.[4,5] Based on a similar geometry, a magnifying hyperlens was fabricated at optical frequencies,[7] where 16 layers of Ag/Al2O3 were used to produce the hyperlens, but large-scale fabrication of such hyperlenses is challenging. The approach was extended to spherical hyperlenses, which magnifies images in two lateral dimensions with resolution beyond the diffraction limit.[8]

At lower frequencies such as THz and microwaves, hyperlenses can be made with wire media (WM).[6] At THz frequencies Tuniz *et al.*,[13] experimentally demonstrated both magnifying and non-magnifying hyperlenses by fabricating a WM with the fiber drawing method.[14] The magnifying hyperlens was produced using a tapered section of the fiber that supports propagation of near-field features below the diffraction limit. However, fabrication of such larger tapers is also challenging. One of the key advantages of WM is that they are robust to fabrication imperfections,[3,15] and have low loss[16] in microwave to THz frequencies.

Hyperlenses rely on either curved geometries or tapering of the medium, which are difficult to manufacture. A prism shape, as originally suggested by Salandrino *et al.*,[4] may be realized by an obliquely cut output interface of a hyperbolic metamaterial, and could be considerably easier to fabricate. A prism in the canalization regime provides a magnified image at the output, where image magnification depends on cutting angle of the output interface. One of the main drawbacks with the prism geometry is that an image is formed at the output surface only – upon leaving the prism, different spatial frequencies are refracted at different angles and the prism cannot be simply used as a magnifying lens in the far-field, as can be done with spherical or tapered hyperlens. Finally, while not considered in the original paper, strong resonant behavior is expected in such a finite structure, which would inevitably lead to imaging artefacts.

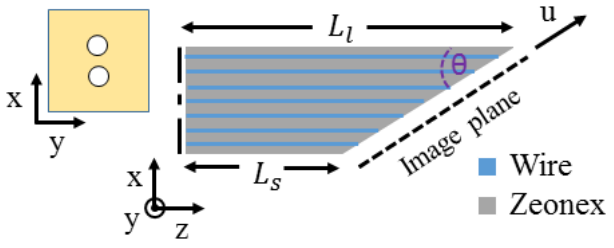

FIG. 1. Schematic of the magnifying wire medium prism. The diameter of the apertures is 200 μm with inner edge-to-edge separation 100 μm.

Recent theoretical and experimental investigation revealed that imaging devices based on WM offer high quality images at the Fabry-Perot resonances (FPRs) of the device, however, away from such resonances images severely deteriorate,[3,17,18]

[a)]Electronic mail: samiul.habib@sydney.edu.au

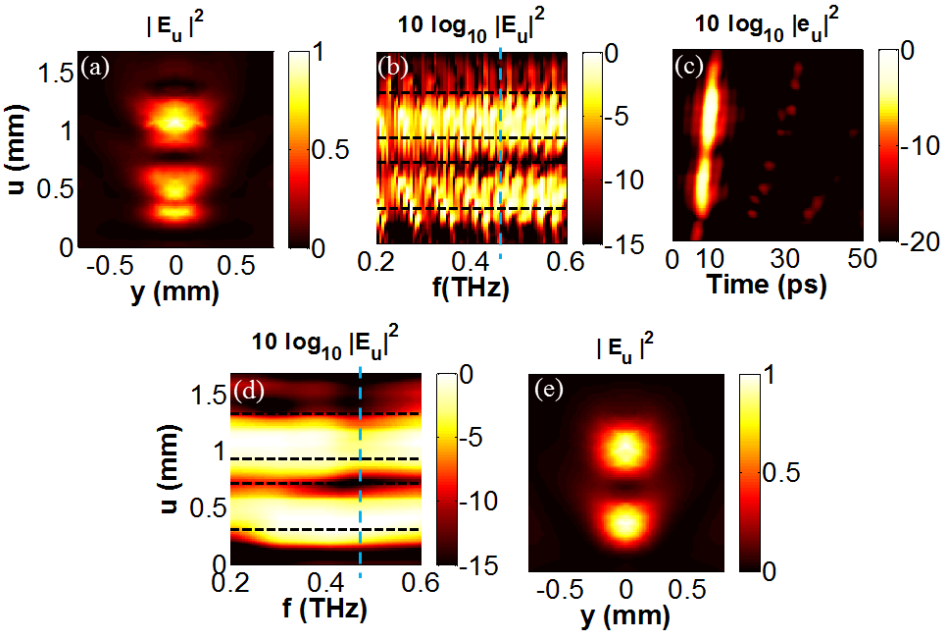

FIG. 2. (a) Simulated intensity of the 2D image at 0.47 THz. (b) Simulated frequency dependent intensity profile along the u-axis through the center (at $y = 0$) of the hyperlens. (c) Temporal intensity profile as a function of position and time (at $y = 0$). (d) Simulated intensity after convolution and (e) Intensity of the 2D image after convolution at 0.47 THz. Horizontal dotted lines in Fig. (b,d) indicate the location of the imaged apertures.

which thus limits the use of such devices for broad-band imaging. Kaltenecker *et al.,*[17] experimentally demonstrated that artefacts appearing when imaging through a straight section of the WM arise from reflections, which can be eliminated by using single-cycle excitation pulses and time resolved measurements. More recently, we reported that such a time gating of ultra-short pulse measurements can be reproduced in the frequency domain using appropriate convolution,[18] resulting in improved images away from FPRs. As we will see, region of high quality images do not necessarily exist in the prism configuration, implying a greater need for an appropriate post-processing.

In spite of the drawbacks, the main advantage of the prism geometry is that it does not rely on curved geometry or tapering, making the structure simpler to fabricate than an equivalent curved or tapered structure operating at the same frequency. To date no experimental results based on such geometry have been reported.

In this letter we present an experimental demonstration of a prism design of magnifying hyperlens based on WM, analogous to the magnifying hyperlens proposed earlier by Salandrino *et al*.[4] We experimentally demonstrate transmission of near-field information and magnification. Our experiments show the existence of imaging artefacts due to reflections from the interfaces. In order to eliminate the reflections, we introduce a spectral convolution technique equivalent to spatially variable time gating that restores the images, enabling the use of the prism hyperlenses for broad-band imaging.

The paper is organized as follows. First, we study the image transmission properties of the hyperlens via numerical simulations, and also present a numerical method to eliminate the artefacts. We then discuss the fabrication method used to produce the WM, and present a simple and inexpensive technique to make the final shape of the hyperlens. Finally, we discuss characterization of the sample and present near-field experimental results.

Figure 1 shows a schematic of the prism design of the magnifying hyperlens. Such geometry allows magnification of the field distribution at the input end by effectively projecting the modes propagating along the WM on the tilted side. Since the output surface is skewed, a magnified image is obtained at the output, and magnification on the output interface can be determined by the ratio between wire spacing at both ends of the device, which is equivalent to the inverse sine of the angle at the tip of the prism, $1/\sin\theta$. The hyperlens considered for the simulations is composed of 153 (17×9) indium wires with 10 μm diameter and 50 μm spacing, surrounded by Zeonex. In the simulations the refractive index of Zeonex is taken to be 1.52.[14] The WM is oriented along the z-axis, and the objects to be imaged are placed in the xy-plane with the features to be resolved aligned on the x axis, see Fig. 1. The prism is designed so that the angle at the tip of the prism is $\theta = 29^0$ and the length corresponding to the long side in the z direction is L_l= 3 mm, consequently making the short side L_s = 1.56 mm. The chosen parameters lead to a length difference between consecutive wires of 90 μm in the z direction, and to a spacing of 102 μm along the image plane, corresponding to a two-fold magnified image at the output interface.

For a straight uniform length WM, the wires all resonate at the same frequencies, but for the prism hyperlens, since the

wires are of different length along the propagation direction, they resonate at different frequencies not having a condition where undistorted images are created as it was at the FPRs for the straight hyperlens. In order to investigate the effect of wire resonances, and how reflections supported by the wires affect imaging quality, we use finite integral based software (CST) as a simulation tool. To reduce the computational time we exploit the symmetry of the geometry and apply perfect magnetic boundary conditions in the *xz*-plane. In our simulation, we consider two sub-wavelength circular apertures (diameter 200 μm and spacing 100 μm), placed 5 μm away from the flat input side (object plane) of the hyperlens, and imaged at the tilted output side (image plane). The electric field is calculated for frequencies between 0.2 and 0.6 THz with 5 GHz steps, which corresponds to a wavelength range of 500 to 1500 μm. The aperture size and separation are thus well below the diffraction limit over most of the frequency range.

The apertures are excited by an *x*-polarized plane wave propagating along the direction of the wires (z), and the electric field is calculated 70 μm away from the output interface. Figure 2(a) shows the simulated intensity of the 2D image at 0.47 THz, which results in a magnified image at the output, but the image is difficult to interpret. One of the aims of this work is to correct the distorted image. To analyze the frequency dependence of the imaging, the intensity in the center of the 2D images ($y = 0$), which is referred to as the line-scan, is plotted as a function of the position on the image plane, (coordinate u in Fig. 1) and frequency, as shown in Fig. 2(b). The intensity is then normalized to the input spectrum. The input spectrum is calculated at the center of one of the bare apertures (without hyperlens). Frequency dependent fields are denoted by upper case **(E)**, while we use lower case **(e)** for temporal fields. In Fig. 2(b), two bands of intensity maxima with location matching the apertures can be seen, however, strong frequency dependent artefacts arising from the different resonant frequencies of the different wires degrade the image.

Here we show that a similar method to that used in our previous work[18] to eliminate artefacts arising from reflections in straight sections of WM can be modified and applied to the prism geometry. To avoid the reflections in the prism geometry, time gating of the ultra-short pulses needs to be adjusted according to the varying lengths of each wire. In the frequency domain, this spatially variable time gating can be achieved by convolving the electric field with a phase shifted sinc function. The electric field, $\boldsymbol{e}'$ of the time gated pulse can be written as[18]

$$\boldsymbol{e}'(t) = \boldsymbol{e}(t)\Pi(\frac{t-t_s}{\tau}) \tag{1}$$

where $\boldsymbol{e}$ represents the electric field and t_s is the time shift corresponding to the varying lengths of each wire. The rectangular function $\Pi(\frac{t}{\tau})$ of Eq. (1) is defined as:

$$\Pi(\frac{t}{\tau}) = \begin{cases} 0; t>\tau, t<0, \\ \frac{1}{2}; t=0, t=\tau, \\ 1; 0<t<\tau, \end{cases} \tag{2}$$

τ denoting the gate width required to avoid reflections. The gating width τ should be longer than the pulse width but shorter than the propagation time of the first reflected pulse. To obtain the fields in the frequency domain we apply the Fourier transform to Eq. (1), which can be written as

$$\boldsymbol{E}'(\omega) = \boldsymbol{E}(\omega) * [\tau \times sinc(\omega\tau/2\pi) \times exp(-i\omega(2t_s+\tau)/2)] \tag{3}$$

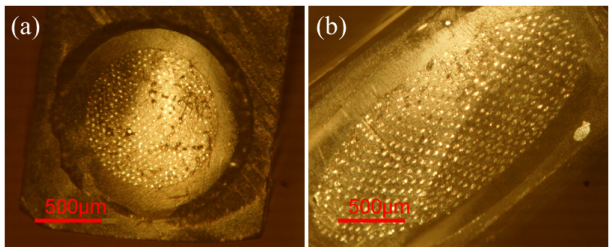

FIG. 3. Microscope image of the fiber cross section (a) input side and (b) output side.

Now, to determine the proper gate width, the temporal intensity profile corresponding to Fig. 2(b) is retrieved by applying a Fourier transform, which is shown in Fig. 2(c). Since wires have unequal length along the output interface, the temporal intensity along the interface (u-line) appears slanted. From the temporal field profile it is possible to see the reflected pulses, where the separation between consecutive reflections is $2nL/c$, where n is the refractive index of Zeonex and c is the speed of light. Figure 2(c) reveals that the first reflection is temporally well separated from the main pulse by 15.0 ± 0.5 ps. Despite the intensity of the first reflected pulse being low ($\sim$14 dB lower than the main pulse), the effect of it on the image quality is not negligible.

In the simulation, the width of the excitation pulse is taken as 4 ps, and to eliminate the reflections, we use a gating pulse width of 7 ps. Such a gating pulse width will not cut the main part the signal. Figure 2(d) shows the intensity profile as a function of frequency after convolution. The frequency dependent artefacts arising from different resonant frequencies have been mitigated after applying the convolution method and the images of the two apertures are now clearly separated over the entire frequency band considered. As an example, the intensity of the 2D image at 0.47 THz after convolution is plotted in Fig. 2(e), showing a significant improvement in the image quality compared with the image before convolution, Fig. 2(a).

Note that, in spite of the fact that convolution gives a better image, the image is elongated in one direction (along y) which is due to the excitation of ordinary waves,[18] the impact of which could also be mitigated by adopting appropriate image processing.[18]

We used a wire medium fabricated previously using the fiber drawing technique, a technique potentially allowing mass production of metamaterials with low cost.[13] The straight section of the WM contains 443 hexagonally arranged indium wires with average diameter and spacing of 10 μm and 50 μm respectively, embedded in Zeonex, a cyclo-olefin polymer with low losses at THz frequencies.[19] The outer diameter of the hyperlens is $\sim$1.3 mm. As a metal, indium is used because it has low melting temperature 156.6^{0}C, which is there-

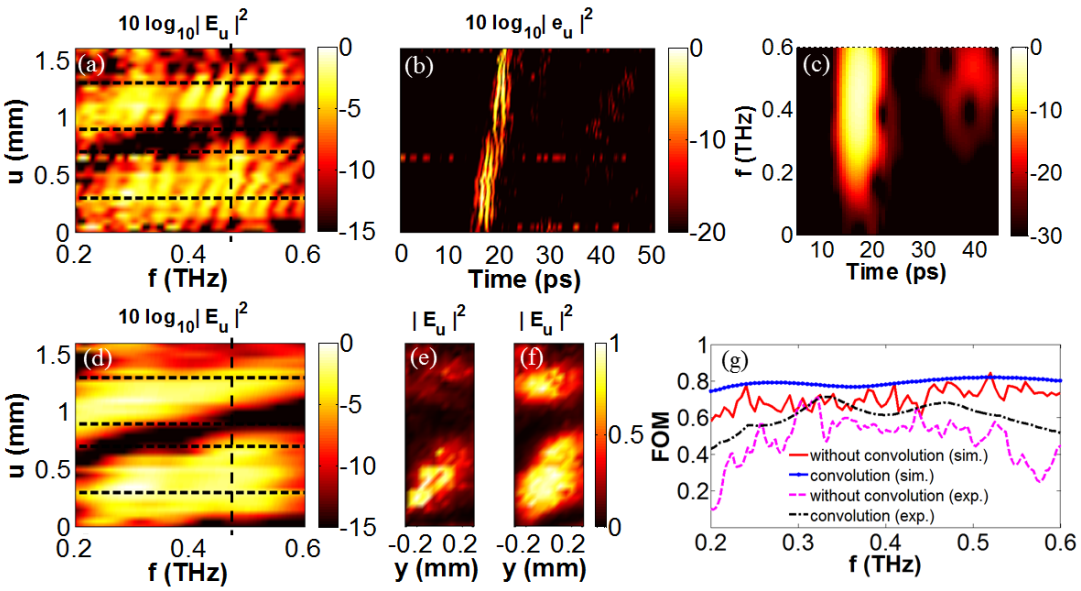

FIG. 4. (a,b) Experimental frequency dependent intensity profile and temporal intensity profile along the u-axis through the center of the hyperlens. (c) Spectrogram of the temporal signal at u = 1.1 mm. (d) Experimental intensity profile after convolution. (e) Intensity of the 2D image at 0.47 THz and (f) after convolution at 0.47 THz. (g) FOM of the raw image and after applying the convolution method as a function of frequency for both simulation and experiment. Horizontal dotted lines in Fig. (a,d) indicate the location of the imaged apertures.

fore suitable for co-drawing with Zeonex.

The prism shaped hyperlens is fabricated as follows. We take a PMMA sheet of thickness ∼2 mm, cut out of it a triangular template with the required angles (mimicking the angled part of the prism), drill a ∼1.5 mm hole in the template, insert the fiber into the hole, and fix it with adhesive so that it composes a single piece with the template. The faces may then readily be polished to the required angles with good flatness. Figure 3 shows microscope images of the fiber cross section at the transversely polished input side and slanted elongated output side. The inner diameter of the input side of the hyperlens is ∼1050 μm, whereas the elongated diameter on the output side is ∼2200 μm. The microscope image shown in Fig. 3 reveals small defects and variation of the wires dimensions over the cross section of the fiber, however, we do not expect these to significantly influence the imaging performance of the hyperlens.

To characterize the transmission properties of the hyperlens, we use time resolved THz time domain spectroscopy. We place two apertures (dimension and separation the same as considered in the simulation) in direct contact with the input side of the hyperlens, illuminate the apertures with x-polarized THz pulses, and measure the projection of the electric field along u (E_u) using a near-field antenna, after propagation through the hyperlens. The detector is moved along the u and y directions, resulting in a pixel-by-pixel raster scan of the near-field. The raster scan is taken over 0.6 mm ×1.6 mm with 0.05 mm steps in both directions. Spectral information is obtained through the Fourier transform of the temporal signal.

Figure 4 shows the experimental results. Figure 4(a) shows the frequency dependent near-field intensity, normalized with the input pulse spectrum, where the input spectrum is measured at the center of one of the bare apertures (without hyperlens). As for the simulations, we see strong signals matching the location of the apertures, indicating that our device can separate feature sizes below the diffraction limit, and provides a two-fold magnified image. However, we also observe distortion of the image at some frequencies, see for example the vertical dotted line in Fig. 4(a) and the corresponding image in Fig. 4(e). Figure 4(b) shows the temporal intensity profile which is slanted as expected. The intensity of the first reflection is very weak (∼16 dB below the main pulse), and the separation between them is 16.0 ± 0.5 ps.

Though the intensity of the first reflected pulse is weak, Fig. 4(a) and (e) show it can nonetheless severely distort the image quality. In order to consider whether the time gating method is applicable, we need to consider broadening of the pulse due to dispersion. In general, when a pulse propagates through a dispersive medium, group velocity dispersion leads to a broadening of the pulse in the time domain, depending on initial pulse width and propagation length. We measure broadening of the main pulse after propagating through the hyperlens at u = 1.1 mm (center of one aperture), giving a full width half maximum of the pulse of 5.0 ± 0.5 ps, which is approximately twice that measured through bare apertures without hyperlens (2.5 ± 0.5 ps). At the longer side of the prism, longer wire lengths lead to increased pulse broadening, but the reflected pulses are then also further delayed proportionally. For these parameters, reflected pulses can thus always be separated from the main pulse. Figure 4(c) shows a spectrogram of the temporal signal at u = 1.1 mm, which provides information on pulse broadening with time and frequency. From Fig. 4(c) it is clear that main pulse is well separated from the first reflected pulse, and the time gating method can be applied.

Applying the same position dependent convolution technique as in the simulation but with a time gating width of 10 ps to allow for the effect of dispersion, results in improved images [Fig. 4(d), (f)]. The convolution eliminates reflections, providing a clear separation of the two apertures over the entire frequency band considered. The raw image at 0.47 THz is plotted in Fig. 4(e), showing a distorted image which is noticeably improved after convolution, Fig. 4(f).

We use a figure of merit (FOM)[18] as a function of frequency, which is calculated by comparing the electric field distribution of the imaged apertures (with hyperlens) to the two ideal rectangular apertures distribution. The FOM is expressed such that a value of 1 indicate that transmission of the near-field of the aperture is perfect. For both simulation and experiment [Fig. 2(b,d) and Fig. 4(a,d)], we calculate the FOM of the raw image, and after applying the convolution method. This is shown in Fig. 4(g) where it may be observed that for both simulation and experiment the FOM of the raw image (without convolution) is fluctuating, and is very low at some frequencies (where the image quality is very poor), indicating that it is difficult to interpret images over a wide range of frequencies. At some frequencies (see peaks of the raw image trace in Fig. 4(g)) it is possible to achieve good images, however, as these frequencies are typically not known a priori this is not very useful. After applying the convolution method, the FOM exhibits a higher value with less fluctuations, meaning better images can be obtained over the entire frequency band considered. The convolution processing provides up to a factor of four improvement in the FOM for the worst raw images, whilst only negligibly degrading the best images.

The geometry investigated requires some considerations on the loss for the fabricated fiber. For the straight section of the fiber, loss was experimentally characterized using the cutback technique to be increasing from 0.8 to 1.8 dB/mm between 0.2 - 0.6 THz.[13] In our device, since the wires are of different lengths, loss will be different along the slanted side of the lens due to the different propagation length. There is a difference in propagation distance of 541 μm between the apertures, and this additional wire length gives a maximum additional loss of 0.65 dB loss, which is not very significant and could easily be compensated. This number would increase for larger hyperlenses, or a similar hyperlens with larger magnification – however, at this stage this doesnt seem to pose a practical limitation.

In conclusion, we have designed, fabricated, and experimentally characterized the near-field transmission of a wire medium prism. The designed structure has the advantage of being a simple design and does not rely on tapering, making fabrication easier. We have experimentally demonstrated that the hyperlens can resolve sub-wavelength features below the diffraction limit and provides a two-fold magnified image at the output. The magnification of the hyperlens can be enhanced by adjusting the prism angle. However, we observed that our device also showed strong imaging artefacts due to reflections, making the resolution of sub-wavelength features difficult. Appropriate post-processing through space dependent convolution or time gating can be used to remove the artefacts.

A drawback of the prism hyperlens is that it magnifies images in one dimension only. A cone geometry might be similarly easy to fabricate and provide magnification in two dimensions. The second drawback of this type of geometry is that while they do convert sub-diffraction details to spatial frequencies that do propagate in free space, they only form a direct image immediately at the output surface. However, in principle the sub-diffraction details can be reconstructed in the far-field, using appropriately designed compensating far-field optics, or through numerical post-processing if measurements include phase.

The authors would like to thank Richard Lwin for providing assistance in PMMA template fabrication. This research was supported by the Australian Research Council (ARC) under the Discovery Project scheme number DP120103942, and partly under the ARC Centre of Excellence scheme CUDOS (CE110001018). A. S. acknowledges the Eugen Lommel Stipend and Marie Sklodowska-Curie grant of the European Unions Horizon 2020 research and innovation programme (708860). S. A. acknowledges a support of ARC funding DE140100614.

[1] D. R. Smith and D. Schurig, Phys. Rev. Lett. **90**, 077405 (2003).
[2] A. Poddubny, I. Iorsh, P. Belov, and Y. Kivshar, Nat. Photon. **7**, 948–957 (2013).
[3] A. Tuniz, D. Ireland, L. Poladian, A. Argyros, C. M. de Sterke, and B. T. Kuhlmey, Opt. lett. **39**, 3286–3289 (2014).
[4] A. Salandrino and N. Engheta, Phys. Rev. B **74**, 075103 (2006).
[5] Z. Jacob, L. V. Alekseyev, and E. Narimanov, Opt. Express **14**, 8247–8256 (2006).
[6] P. Ikonen, C. Simovski, S. Tretyakov, P. Belov, and Y. Hao, App. Phy. Lett. **91**, 104102 (2007).
[7] Z. Liu, H. Lee, Y. Xiong, C. Sun, and X. Zhang, Science **315**, 1686 (2007).
[8] J. Rho, Z. Ye, Y. Xiong, X. Yin, Z. Liu, H. Choi, G. Bartal, and X. Zhang, Nat. Comm. **1**, 1148 (2010).
[9] Y. Zhao, G. Palikaras, P. A. Belov, R. F. Dubrovka, C. R. Simovski, Y. Hao, and C. G. Parini, New. J. Phy. **12**, 103045 (2010).
[10] J. Sun, M. I. Shalaev, and N. M. Litchinitser, Nat. Comm. **6**, 7201 (2015).
[11] G. Shvets, S. Trendafilov, J. B. Pendry, and A. Sarychev, Phys. Rev. Lett. **99**, 053903 (2007).
[12] A. V. Kildishev and E. E. Narimanov, Opt. Lett. **32**, 3432–3434 (2007).
[13] A. Tuniz, K. J. Kaltenecker, B. M. Fischer, M. Walther, S. C. Fleming, A. Argyros, and B. T. Kuhlmey, Nat. Comm. **4**, 2706 (2013).
[14] A. Tuniz, B. Kuhlmey, R. Lwin, A. Wang, J. Anthony, R. Leonhardt, and S. Fleming, App. Phy. Lett. **96**, 191101 (2010).
[15] C. R. Simovski, P. A. Belov, A. V. Atrashchenko, and Y. S. Kivshar, Adv. Mater. **24**, 4229–4248 (2012).
[16] P. A. Belov, Y. Hao, and S. Sudhakaran, Phys. Rev. B **73**, 033108 (2006).
[17] K. J. Kaltenecker, A. Tuniz, S. C. Fleming, A. Argyros, B. T. Kuhlmey, M. Walther, and B. M. Fischer, Optica **3**, 458–464 (2016).
[18] M. S. Habib, A. Tuniz, K. J. Kaltenecker, Q. Chateiller, I. Perrin, S. Atakaramians, S. C. Fleming, A. Argyros, and B. T. Kuhlmey, Opt. Express **24**, 17989–18002 (2016).
[19] J. Anthony, R. Leonhardt, A. Argyros, and M. C. Large, J. Opt. Soc. Am. B **28**, 1013–1018 (2011).